The variable Crab Nebula

Marco Tavani[*][†]

INAF-IASF-Rome and University of Tor Vergata, Rome (Italy)

E-mail: tavani@iasf-roma.inaf.it

The remarkable Crab Nebula is powered by an energetic pulsar whose relativistic wind interacts with the inner parts of the Supernova Remnant SN1054. Despite low-intensity optical and X-ray variations in the inner Nebula, the Crab has been considered until now substantially stable at X-ray and gamma-ray energies. This paradigm has been shattered by the AGILE discovery in September 2010 of a very intense transient gamma-ray flare of nebular origin. For the first time, the Crab Nebula was "caught in the act" of accelerating particles up to 10^{15} eV within the shortest timescale ever observed in a cosmic nebula (1 day or less). Emission between 50 MeV and a few GeV was detected with a quite hard spectrum within a short timescale. Additional analysis and recent Crab Nebula data lead to identify a total of four major flaring gamma-ray episodes detected by AGILE and *Fermi* during the period mid-2007/mid-2011. These observations challenge emission models of the pulsar wind interaction and particle acceleration processes. Indeed, the discovery of fast and efficient gamma-ray transient emission from the Crab leads to substantially revise current models of particle acceleration.

25th Texas Symposium on Relativistic Astrophysics - TEXAS 2010
December 06-10, 2010
Heidelberg, Germany

---

[*]Speaker.

[†]Report presented on behalf of the AGILE Team.

1. The context

The Crab Nebula is probably the most studied source in high-energy astrophysics. It is at the center of the SN1054 supernova remnant, and consists of a rotationally-powered pulsar interacting with a surrounding nebula through a very powerful relativistic wave/particle wind (e.g., refs. [43, 31]). Many observations and theoretical modelling were devoted to the study of this remarkable system. A powerful pulsar located at its center (of spindown luminosity L_{PSR}= $5\cdot10^{38}$ erg s^{-1}, and spin period P = 33 ms) is energizing the whole system with its wave/particle output. The Nebula and its pulsar emit unpulsed and pulsed emission, respectively, in a broad-band spectrum ranging from radio to TeV energies. The Crab is then an ideal laboratory to study very efficient particle acceleration subject to the different physical conditions of the following sites: (**S1**) the pulsar magnetosphere, (**S2**) the relativistic pulsar wind, (**S3**) the relativistic termination shocks, (**S4**) MHD and/or plasma flow instabilities, (**S5**) large-scale nebular interactions.

The inner Nebula shows distinctive and variable optical and X-ray brightness enhancements ("wisps", "knots", and the "anvil" aligned with the pulsar "jet") [45, 31, 29, 30, 55]. Time variations of these features (weeks, months) have been attributed to local enhancements of the synchrotron emission related to instabilities and/or shocks in the pulsar wind outflow. These variations are indicative of changing acceleration tied to the physical processes originating especially in sites S3 and S4. However, this variable local activity in the inner Nebula, remarkable as it is [29, 30], has been known to produce only small percentage variations of the total Crab radio, optical, X-ray and gamma-ray energy fluxes. It is not surprising that, when averaged over the whole inner region (several arcminute across), the Crab Nebula has been considered essentially stable, and used as a "standard candle" in high-energy astrophysics.

Synchrotron and inverse Compton modelling of the Crab Nebula emission produces a reasonable picture of its *average* properties (e.g., [43, 32, 18, 19, 7, 6, 37]]). The MHD pulsar wind interacts with its environment through a sequence of "shocks" or dissipation features localized at distances larger than a few times 10^{17}cm. Particle acceleration processes (mostly in the pulsar wind and termination shock regions) produce at least two main populations of accelerated electrons/positrons that explain the radio/optical and the X-ray/gamma-ray emissions, respectively [19, 7, 37]. The optical/radio and the X-ray continuum and gamma-rays up to $\sim 50-100\,$MeV energies are modelled by synchrotron radiation of accelerated particles in an average nebular magnetic field $\bar{B} = 200\,\mu$G [29, 19, 7, 37]. Radiation from GeV to TeV energies is modelled as the sum of different contributions of inverse Compton components of electrons/positrons scattering CMB and nebular soft photons [18, 19, 7, 37].

Acceleration at the pulsar wind termination shock regions S3 is crucial for our purposes. The Kennel-Coroniti analysis of the Nebula indicating a low-sigma pulsar wind [32] favors "strong" shocks at S3. Different acceleration models have been proposed, including diffusive processes (e.g., [14, 18, 19, 7]), shock-drift acceleration (e.g., Begelman & Kirk 1990) or ion-mediated acceleration (e.g., [6, 46]). In general, diffusive acceleration models imply acceleration rates of order of the relativistic electron cyclotron frequency ω_B/γ (with $\omega_B = eB/m_e c$, and γ the electron's Lorentz factor), that is $\tau_{acc} \simeq \alpha' \omega_B/\gamma = c/R_L$ with $\alpha' \leq 1$ an efficiency parameter and R_L the Larmor radius (e.g., [18, 19, 7]). If we assume: (i) a Doppler factor $\delta = \Gamma^{-1}(1-\beta\cos(\theta))^{-1} = 1$ (with θ the emission angle with respect to the line of sight), (ii) $\alpha' \simeq 1$, (iii) the equality between the

accelerating electric field (E) and the magnetic field at the acceleration site, and (iv) synchrotron cooling in the co-spatial magnetic field, we obtain a most quoted constraint for the maximum radiated photon energy $\varepsilon_{\gamma,max}$ [18, 19]

$$\varepsilon_{\gamma,max} \simeq \frac{m_e c^2}{\alpha} \simeq 50 \, \text{MeV} \tag{1.1}$$

with $\alpha = e^2/\hbar c$ the fine structure constant, c the speed of light, and m_e the electron's mass. Eq. 1.1 applies in a natural way to particles "slowly" accelerated, e.g., by diffusive processes, and $E_{\gamma,max}$ turns out to be independent of the local magnetic field. The quasi-exponential cutoff shown by the average Crab Nebula gamma-ray spectrum in the 10 MeV - 10 GeV range supports this idealization [18, 19]. However, the local equality between the electric and magnetic fields (expected in MHD models and/or electromagnetic turbulent wave heating) should not be imposed. Considering also the possible effects of a non-trivial Doppler factor $\delta \neq 1$ and acceleration efficiency $\alpha' \neq 1$, the most general expression for the maximum synchrotron-emitted photon energy is[1]

$$\varepsilon_{\gamma,max} \simeq \frac{9}{4} \left(\frac{E}{B} \right) \frac{m_e c^2}{\alpha} \left(\frac{\delta \, \alpha'}{\langle \sin(\theta') \rangle} \right) \simeq (150 \, \text{MeV}) \left(\frac{E}{B} \right) \left(\frac{\delta \, \alpha'}{\langle \sin(\theta') \rangle} \right) \tag{1.2}$$

where $\langle \sin(\theta') \rangle$ takes into account the effects of the average pitch angle θ'. We expect the combination $\delta \, \alpha'/\langle \sin(\theta') \rangle$ to be of order unity as confirmed by the average steady emission of the Crab Nebula showing the "synchrotron burn-off" above 10 MeV [19]. Expectations from MHD-based models of emission are clear, and well represented by Eq. 1.2. This theoretical framework is now challenged by the AGILE discovery of the strong gamma-ray flare from the Crab Nebula in September 2010 [50, 51], as we describe below.

2. The discovery

The AGILE satellite [49] observed the Crab Nebula several times both in pointing mode from mid-2007/mid-2009, and in spinning mode starting in November 2009. The AGILE instrument monitors cosmic sources in the energy ranges 50 MeV - 10 GeV (hereafter, GeV gamma-rays) and 18 - 60 keV with good sensitivity and angular resolution. With the exception of occasional flaring episodes (see below), AGILE detects an average (pulsar +nebula) flux value $F_{ave} = (2.2 \pm 0.1) \times 10^{-6} \, \text{ph cm}^{-2} \, \text{s}^{-1}$ in the range 100 MeV - 5 GeV [41], for an average photon index $\alpha = 2.13 \pm 0.07$.

During routine monitoring in spinning mode in September 2010, a strong and unexpected gamma-ray flare from the direction of the Crab Nebula was discovered by AGILE above 100 MeV and immediately reported to the community [50]. The flare reached its peak during 19-21 September 2010 with a 2-day flux of $F_{g,p1} = (7.2 \pm 1.4) \times 10^{-6} \, \text{ph cm}^{-2} \, \text{s}^{-1}$ ($\alpha = 2.03 \pm 0.18$) for a 4.8 s.d. detection above the average flux. The flux subsequently decayed within 2-3 days to normal average values (Fig. 1) [51]. This flare was confirmed within 1 day by *Fermi*-LAT [15], and different groups obtained multifrequency data during the days immediately following the flare (see ref. [12] for a summary of follow-up observations). Recognizing the importance of this event was facilitated by a previous AGILE detection of the Crab Nebula with similar characteristics. Indeed,

---

[1]See also ref. [5].

AGILE detected another remarkable flare from the Crab in October, 2007 (see also [41]). This flare lasted ∼2 weeks and showed an interesting time sub-structure (Fig. 2, top panel). The peak flux was reached on Oct. 7, 2007, and the 1-day integration value was $F_{g,p2} = (8.9 \pm 1.1) \times 10^{-6} \, \mathrm{ph \, cm^{-2} \, s^{-1}}$ ($\alpha = 2.05 \pm 0.13$) for a 6.2 s.d. detection above the standard flux.
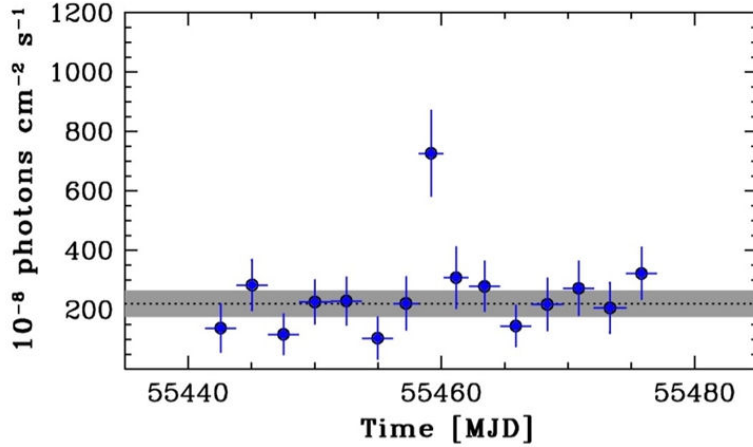

Figure 1: The AGILE gamma-ray lightcurve of the Crab pulsar + nebula above 100 MeV showing the September 2010 flare [51]. The band marked in grey shows the average flux within 3 standard deviations.

The pulsed emission from the Crab pulsar is characterized very well from radio, optical, X-ray up to gamma-ray energies [24, 1, 40]. For all major flares and especially for the October 2007 and September 2010 events there was no sign of variation of the pulsar signal before, during and after these flares (e.g., supplemental information in [51]). For the Sept. 2010 event the issue of search for possible variation of the pulsed emission was thoroughly studied at radio [22], X-ray [51] and gamma-ray [26, 2, 51] energies. Thus, we attribute the major gamma-ray flares from the Crab to transient emission originating from relativistic particles accelerated in the inner Nebula, or in regions decoupled from the rotating magnetosphere producing the pulsed emission[2].

3. Major gamma-ray flares

Four major gamma-ray flaring episodes from the Crab Nebula have been reported during the period mid-2007/mid-2011 by AGILE [51, 52, 47, 48] and *Fermi*-LAT [2, 16, 27] (see Table 1).

---

[2]There is no evidence for an additional extra transient source (flaring blazar or Galactic source) near the Crab Nebula for the Sept. 2010 event or for other major gamma-ray flares. A typical Crab Nebula gamma-ray error box radius for long integrations is $r = 0.1^o$ or less, for both AGILE and *Fermi*-LAT (e.g., [1]). In particular, for the September 2010 event no change in the hard X-ray flux was detected by Integral and Swift/BAT [23, 38], and no other X-ray source was detected by *Swift*/XRT about 3 days after the event (0.7 mCrab upper limit for a source in an annular region of size between 1 and 2 arcminutes, and 0.3 mCrab upper limit in an annular region of radius between 3 and 10 arcminutes, [28]). The peculiar flaring gamma-ray spectra and the very high intensity reached in 2010 and 2011 makes the hypothesis of a background transient source even more improbable. Depending on assumptions, the probability or a random occurrence of a peculiar transient source in the Crab Nebula gamma-ray error box is in the range $10^{-4} - 10^{-6}$ [1, 51].

4

The event characteristics and total radiated energies differ from one event to the other. The first two events (in 2007 and 2009) are relatively "slow" in their risetime (a few days) and in the overall temporal evolution. Their duration is at least 2 weeks and the total gamma-ray radiated energy is $E_\gamma \sim 10^{42}$ ergs. The third event (Sept. 2010) detected by both AGILE and *Fermi*-LAT developed on a faster timescale. Its risetime is less than 1 day [51], and the (conservative) lightcurves published by the AGILE and *Fermi*-LAT teams do not show significant emission beyond 4 days. However, there is evidence that the temporal structure of the Sept. 2010 event may be non-trivial as suggested by an analysis of *Fermi*-LAT data [8] that has been recently confirmed by AGILE [48]. The Sept. 2010 event shows variability on a 12-hr timescale with a strong variation of the gamma-ray flux. In this case, the total gamma-ray radiated energy is $E_\gamma \sim 10^{41}$ ergs.

Even more dramatic time variability has been recently detected in the most recent and remarkable Crab flaring event of April, 2011 [16, 52, 27, 47]. In this case, variability at the level of a few hours (and possibly less) has been determined [48, 27]. The April 2011 event can be called a Crab gamma-ray "super-flare", with the flux above 100 MeV reaching the record-high peak of $F = (30 \pm 6) \times 10^{-6} \, \mathrm{ph\,cm^{-2}\,s^{-1}}$ on a 12-hour timescale [48]. This event lasts about 1 week and the total energy emitted above 100 MeV is $E_\gamma \sim 10^{42}$ ergs.

Fig. 3 shows the result of the AGILE long baseline gamma-ray monitoring of the Crab Nebula from mid-2007 until May, 2011 together with the Feb. 2009 flare detected by *Fermi*-LAT. It is interesting to note that all three events appear to be characterized by a "precursor" (lasting a few days) that anticipates a major peak flare. The Crab Nebula is producing major gamma-ray flares with an apparent rate of (1-2)/year. Occasionally, the level of gamma-ray emission is surprisingly high, reaching the level of the brightest gamma-ray blazars. In April, 2011 the Crab Nebula became for a few days the most powerful source in the GeV gamma-ray sky, exceeding the Vela pulsar flux by a factor of almost three !

Table 1: Major gamma-ray flares of the Crab Nebula

Flare date	Duration	Peak flux (*) (pulsar + nebula)	Instrument	Ref.
October 2007	~ 15 days	$9 \times 10^{-6} \, \mathrm{ph\,cm^{-2}\,s^{-1}}$	AGILE	[51]
February 2009	~ 15 days	$7 \times 10^{-6} \, \mathrm{ph\,cm^{-2}\,s^{-1}}$	*Fermi*-LAT	[2]
September 2010	~ 4 days	$7 \times 10^{-6} \, \mathrm{ph\,cm^{-2}\,s^{-1}}$	AGILE, *Fermi*-LAT	[51, 2]
April 2011	~ 10 days	$30 \times 10^{-6} \, \mathrm{ph\,cm^{-2}\,s^{-1}}$	AGILE, *Fermi*-LAT	[16, 52, 27, 47]

* Average peak fluxes obtained for different integration times: 1 day (October 2007), 4 days (February 2009), 2 days (September 2010), 12 hours (April 2011).

4. Modelling the flaring gamma-ray spectrum

Very important information about the Crab inner nebula physical processes can be gained from the flaring spectral data. Fig. 4 shows the published 2-day averaged AGILE spectrum and the 4-day *Fermi*-LAT spectrum of the Sept. 2010 event. Fig. 5 shows the spectrum of the remarkable April 2011 record-high flare [48]. The Crab flare gamma-ray emission above 100 MeV apparently violates Eqs. 1.1 and 1.2, and we need to consider emission models different from those applicable

to the average nebular emission. Standard theories based on MHD modelling with $E/B \leq 1$ and $\delta \sim 1$ can be applied to the average emission, but not to the flaring states. This is a challenge for particle acceleration models that in their standard forms are either too slow (e.g., diffusive models [14, 13, 21]), not sufficiently efficient [33, 44], or not directly applicable for the probable lack of ions [6] in specific sites of the polar jet regions such as the "anvil". Relatively large scale MHD instabilities (e.g., [34, 35, 20, 17]) can play a role in setting the local conditions for fast acceleration, but the current modelling does not capture the flaring acceleration properties that most likely require a detailed kinetic approach. Thus the Crab flaring data may force us to substantially revise previously proposed models of particle acceleration and emission . We notice here the relevance of the possible role of impulsive particle acceleration in magnetic field reconnection, and/or runaway particle acceleration by transient electric fields violating the condition $E/B < 1$. The applicability of these concepts to the Crab Nebula flaring activity remains to be tested by future investigations.

In order to model the observed flare spectra, we assume that a sub-class of the overall particle population in the inner nebula is subject to an impulsive acceleration process at a specific site. In principle, favorably Doppler-boosted emission with $\delta \sim 5 - 10$ might explain some properties of the gamma-ray spectra of Figs. 4 and 5. However, it is not clear whether this large Doppler boosting is supported by the Crab Nebula data and geometry (for a discussion, see ref. [35]). Alternately, a particle acceleration mechanism with and "effective" $E/B \geq 1$ and $\delta \sim 1$ seems to be required. An example of theoretical modelling of the spectral evolution is shown in Fig. 4 for the Sept. 2011 event [54]. Our modelling (aimed at testing the compatibility for this event of the AGILE and *Fermi*-LAT spectra within a synchrotron cooling model) assumes an emitting region of size $L = 7 \times 10^{15}$ cm, and an enhanced local magnetic field $B_{loc} = 10^{-3}$ G. The acceleration process produces, within a timescale shorter than any other relevant timescale, a particle energy distribution that we model as a double power-law distribution [51], $dn/d\gamma = K \gamma_b^{-1}/[(\gamma/\gamma_b)^{p_1} + (\gamma/\gamma_b)^{p_2}]$, where n is the particle number density, $p_1 = 2.1$, $p_2 = 2.7$, $\gamma_b = 2 \times 10^9$, and K a normalization factor. The particle Lorentz factor γ ranges from $\gamma_{min} = 10^6$ and $\gamma_{max} = 7 \times 10^9$. This double power-law distribution implies maximal synchrotron emission between the Lorentz factors γ_b and γ_{max}. The total particle number required to explain the flaring episode turns out to be $N_{e-/e+} = \int dV (dn/d\gamma) d\gamma = 2 \times 10^{42}$, where V is an assumed spherical volume of radius L. Curves labelled in red color and in green color in Fig. 4 mark the results of the model calculation for 2-day and 4-day integrations, respectively. AGILE and *Fermi*-LAT data of the Sept. 2010 event, despite their different integration timescales, are consistent with the rapid synchrotron cooling model of ref. [54].

Fig. 5 shows the even more dramatic peak flaring spectrum of the April 2011 event (from ref. [48]). Spectral modelling of this event requires more extreme values of the physical parameters compared to those applicable for the September 2010 event. In particular, the hour-timescale variability [47, 27] requires very efficient acceleration and fast synchrotron cooling that has to occur for values of the local magnetic field $B_{loc} \geq 1$ mG. A strong amplification of the local magnetic field is then a clear signature of the highly transient acceleration process at work (relativistic shocks, magnetic field reconnection, plasma instabilities). Unveiling the fundamental process of fast acceleration with extreme physical requirements is a challenging opportunity for future theoretical work on the Crab.

5. Chasing the acceleration site

The range of the gamma-ray emission timescales (hours-days), and the extreme energetics of the flaring phenomenon (reaching gamma-ray luminosities of $L_{\gamma,p} = (0.5 - 1) \times 10^{36}$ erg s^{-1} above 100 MeV) indicate an emission site in the inner Crab Nebula. Several regions can be considered for the flaring particle acceleration site including: (1) the South-East polar jet region and in particular the "anvil" site [51, 2] (near the "knot-2" of ref. [45, 29]); (2) the inner ring (visible at the optical and X-ray energies) marking the pulsar wind termination shock; (3) the optical feature very close (~ 0".6) to the pulsar (possibly a standing shock) classified as "knot-1" [35]. High-resolution optical and X-ray observations of the inner Nebula are necessary to address this issue. Fig. 6 shows the results of *Hubble Space Telescope* optical and *Chandra* X-ray observations of the inner Crab Nebula following the Sept. 2010 gamma-ray flare [51]. These observations were obtained 7 to 10 days after the event, and show several active regions both in the optical and in the X-ray energy bands. In particular, the "anvil" region seems brightened compared to other historical observations of the Nebula showing a less prominent emission. Several spots of enhanced X-ray emission (especially those marked as "source-A" and "source-B" in Fig. 6) can be noticed. Several local transient enhancements of optical and X-ray emission have been recorded in that region. They typically last a few weeks, fade, and are back in an apparently random fashion after several months. It is tantalizing to speculate that these features are associated with the fast particle acceleration site producing the major Crab gamma-ray flares, but the current data do not provide a "smoking gun" yet. A program of X-ray monitoring of the Crab inner nebula by *Chandra* started in October 2010 envisioning regular observations about 1 per month to provide an extensive baseline [56]. *Chandra* observed the Crab Nebula several times in coincidence with the super-flare of April 2011 [53]. These observations are currently being analyzed.

6. Conclusions

The Crab Nebula continues to surprise us providing invaluable information on the most extreme acceleration processes. The pattern of well established gamma-ray flares shows a recurrence of about 1-2 events per year, leaving open the possibility that lower level gamma-ray enhanced emission can be produced between major flares. The discovery of this remarkable phenomenon can be attributed to the monitoring capabilities of the current gamma-ray missions, AGILE and *Fermi*. Crab gamma-ray flares are not that rare, and we may wonder why this phenomenon was not discovered earlier. The situation regarding the overall variability in the Nebula is even more interesting today after the recognition that the total X-ray flux from the Crab is subject to long timescale variations of order of years [57]. It is not clear at present whether there is any connection between the pattern of year-long X-ray variations [42] and the fast and intense gamma-ray flaring. If the central pulsar powerhouse determines a variable particle flux over a long timescale, the high-energy activity we witness in the Nebula can be ultimately traced back to the pulsar. Alternately, plasma instabilities favored by large scale MHD flow variations and/or magnetic field reconnection events can lead to the very fast particle acceleration we require to explain the observations. Future HST and Chandra observations of the inner Nebula will be crucial to localize the particle acceleration site. We also note that future TeV observations of the Crab will be important to test

Doppler-boosted models of emission [48]. A claim for transient TeV emission in coincidence with the Sept. 2010 event [3] was not confirmed by independent short (20 min.) observations [39, 36]. However, in light of the fast variability recently determined in the Crab gamma-ray flares, this issue needs to be addressed by future investigations [48]. For sure, we can anticipate in the next years a revival of theoretical and observational investigations of our beloved Crab.

7. Acknowledgements

References

[1] Abdo, A.A. *et al.*, 2010, Astrophys. J., **708**, 1254.

[2] Abdo, A.A., *et al.*, 2011, Science, **331**, 739.

[3] Aielli, G., *et al.*, 2010, Astron. Telegram **2691**.

[4] Aharonian, F.A., 2004, *Very high energy cosmic gamma radiation*, (World Scientific Publishing, ISBN 981-02-4573-4).

[5] Aharonian, F.A., 2011, talk at the ICRANET Workshop, Pescara, March 2011.

[6] Arons, J., 2008, *Pulsars: progress, problems and prospects*, Springer Lecture Notes. ŞNeutron Stars and Pulsars, 40 years after the discoveryŤ, (ed. W. Becker).

[7] Atoyan, A.M. & Aharonian, F.A., 1996, MNRAS, **278**, 525.

[8] Balbo, M., Walter, R., Ferrigno, C. & Bordas, P., 2011, A&A, **527**, 44.

[9] Bednarek, W. & Idec, W., 2011, MNRAS, published online 21 April 2011, doi:10.1111/j.1365-2966.2011.18539.x.

[10] Begelman, M.C. & Kirk, J.C., 1990, ApJ, **353**, 66.

[11] Bell, A.R., 1978, MNRAS, **182**, 147.

[12] Bernardini, E., 2011, Science, **331**, 686.

[13] Blandford, R. & Ostriker, J.P., 1978, ApJ, **221**, L29.

[14] Blandford, R. & Eichler, D., 1987, Phys. Rep. 154, 1

[15] Buehler, R., *et al.*, 2010, Astron. Telegram **2861**.

[16] Buehler, R., *et al.*, 2011, Astron. Telegram **3276**.

[17] Camus, N.F., Komissarov, S.S., Bucciantini, N. & Hughes, P.A., 2009, MNRAS, **400**, 1241.

[18] de Jager O.C. & Harding, A.K., 1992, Astrophys. J., **396**, 161.

[19] de Jager, O.C. *et al.*, 1996, Astrophys. J., **457**, 253.

[20] Del Zanna, L., Amato, E. & Bucciantini, N., 2004, A&A, **421**, 1063.

[21] Drury, L.O., 1983, Rep. Prog. Phys., **46**, 973.

[22] Espinoza, C.M., et al., 2010, Astron. Telegram **2889**.

[23] Ferrigno, C., et al., 2010, Astron. Telegram **2856**.

[24] Fierro, J.M., et al., 1998, Astrophys. J., **494**, 734.

[25] Gallant, Y.A. & Arons, J., 1994, Astrophys. J., **435**, 230.

[26] Hays, E., et al., 2010, Astron. Telegram **2879**.

[27] Hays, E., *et al.*, 2011, Astron. Telegram **3284**.

[28] Heinke, C.O., 2010, Astron. Telegram **2868**.

[29] Hester, J.J., P. A. Scowen & R. Sankrit *et al.*, 1995, Astrophys. J., **448**, 240.

[30] Hester, J.J., Mori, K., Burrows, D. *et al.*, 2002, Astrophys. J., **577**, L49.

[31] Hester, J.J., 2008, Annual Rev. Astron. Astrophys., **46**, 127.

[32] Kennel, C.F. & Coroniti, F.C., 1984, Astrophys. J., **283**, 710.

[33] Kirk, G.J., Guthmann, A.W., Gallant, Y.A., Achteberg, A., 2000, Astrophys. J., **542**, 235.

[34] Komissarov, S.S. & Lyubarsky, Y.E., 2004, MNRAS, **349**, 779.

[35] Komissarov, S.S. & Lyutikov. M., 2011, MNRAS, published online 12 April 2011,
      doi:10.1111/j.1365-2966.2011.18516.x.

[36] Mariotti, M., *et al.*, 2010, Astron. Telegram *2967*.

[37] Meyer, M., Horns, D. & Zechlin, H.S., 2010, A&A, **523**, A2.

[38] Markwardt, C.B., et al., 2010, Astron. Telegram **2858**.

[39] Ong, R.A., *et al.*, 2010, Astron. Telegram **2968**.

[40] Pellizzoni, A., et al., 2009, Astrophys. J., **691**, 1618.

[41] Pittori, C., *et al.*, 2009, Astron. & Astrophys., **506**, 1563.

[42] Qiang, Y.,*et al.*, 2011, Astrophys. J., **730**, L15.

[43] Rees, M.J. & Gunn, J.E., 1974, Mon. Not. R. Astron. Soc., **167**, 1.

[44] Reville, B. & Kirk, J.G., 2010, Astrophys. J., **724**, 1283.

[45] Scargle, J.D., 1969, Astrophys. J., **156**, 401.

[46] Spitkovsky, A. & Arons, J., 2004, Astrophys. J., **603**, 669.

[47] Striani, E., *et al.*, 2011, Astron. Telegram **3286**.

[48] Striani, M., *et al.*, 2011, submitted to ApJ Letters.

[49] Tavani, M., *et al.*, 2009, Astron. Astrophys., **502**, 995.

[50] Tavani, M. *et al.*, 2010, Astron. Telegram **2855**.

[51] Tavani, M., *et al.*, 2011, Science, **331**, 736.

[52] Tavani, M., *et al.*, 2011, Astron. Telegram **3282**.

[53] Tennant, A., *et al.*, 2011, Astron. Telegram **3283**.

[54] Vittorini, V., *et al.*, 2011, ApJ Letters, in press.

[55] Weisskopf, M.C., Hester, J.J., A. F. Tennant, R. F. Elsnor, N. S. Schulz *et al.*, 2000, ApJ, **536**, L81.

[56] Weisskopf, M.C., 2011, private communication.

[57] Wilson-Hodge, C.A., *et al.*, 2010 arXiv:1010.2679v1.
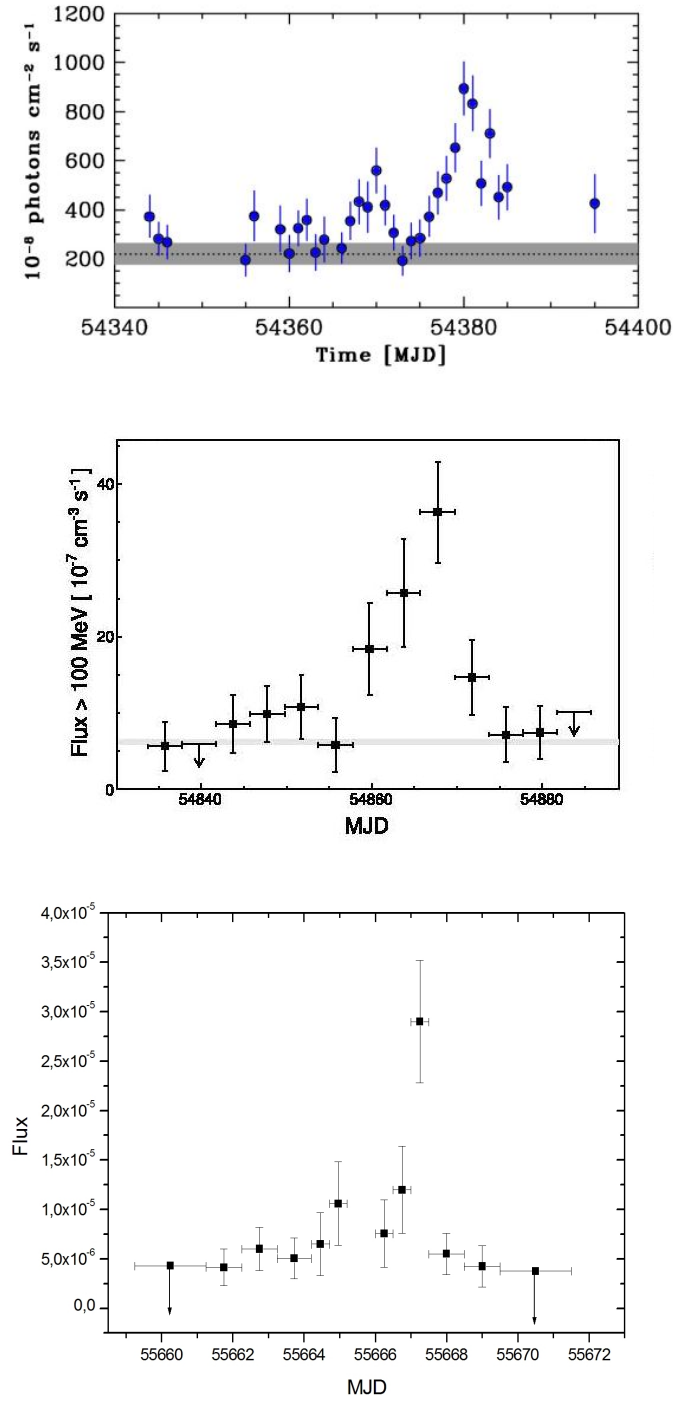
Figure 2: *Upper panel:* the gamma-ray lightcurve of the Crab pulsar + nebula above 100 MeV showing the October, 2007 flare detected by AGILE [51]. The band marked in grey shows the average flux within 3 s.d. *Middle panel:* the gamma-ray lightcurve of the Crab nebula above 100 MeV showing the February, 2009 flare detected by *Fermi*-LAT [2]. The band marked in grey shows the average Nebula flux in the *Fermi*-LAT energy range. *Lower panel:* gamma-ray lightcurve of the Crab pulsar + nebula above 100 MeV showing the October, 2007 flare detected by AGILE [48].
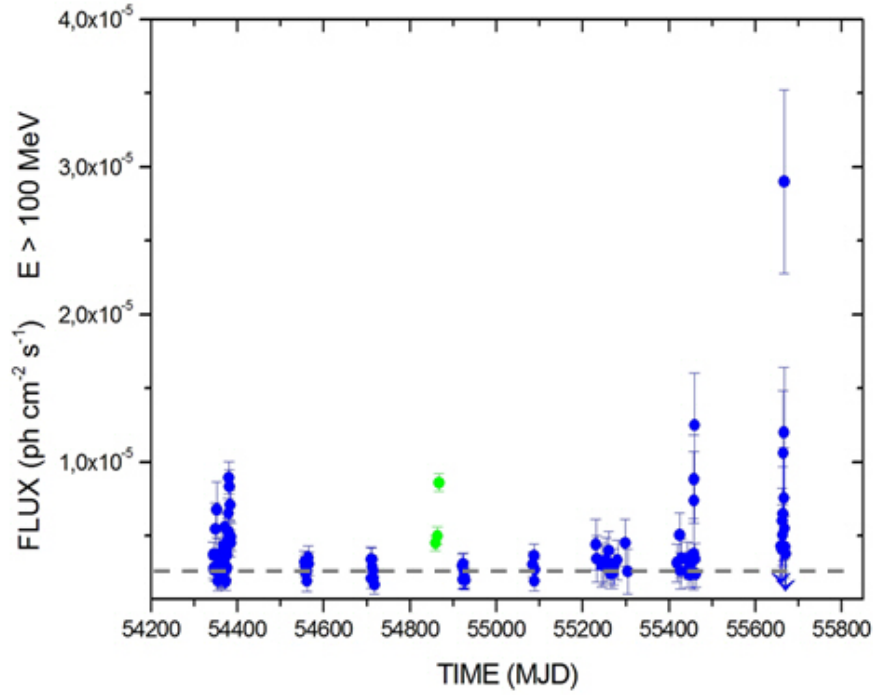
Figure 3: The AGILE gamma-ray lightcurve of the Crab Nebula (pulsar plus nebula) above 100 MeV monitored from mid-2007 until May 2011. The data points marked in green show the gamma-ray flare reported by *Fermi*-LAT [2]. The dashed line marks the average flux in the AGILE-GRID energy range.
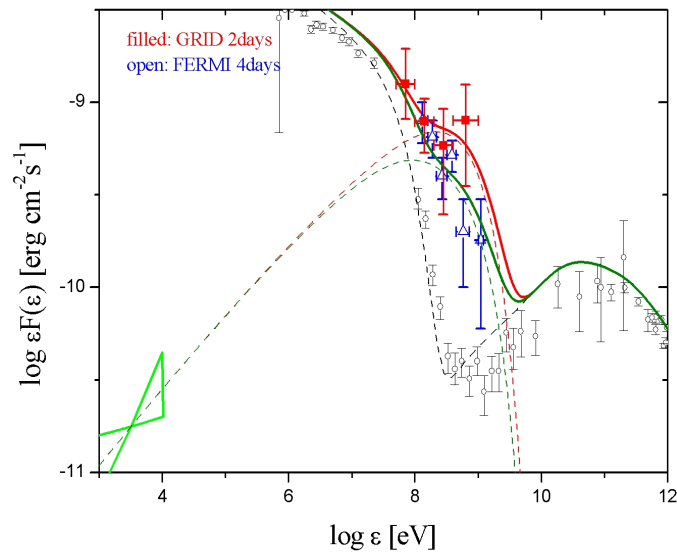

Figure 4: Gamma-ray (pulsar subtracted) spectra of the Crab Nebula September 2010 flare. Red data: AGILE spectrum integrated over a 2-day interval [51]. Blue data: *Fermi*-LAT spectrum integrated over a 4-day interval [2]. Note the different integration times. Black data points show the standard Crab Nebula spectrum [37]. The area marked in green shows the X-ray emission spectrum detected by Chandra about 1 week after the Sept. 2010 flare from "Source A" in the inner Nebula as reported in ref. [51].
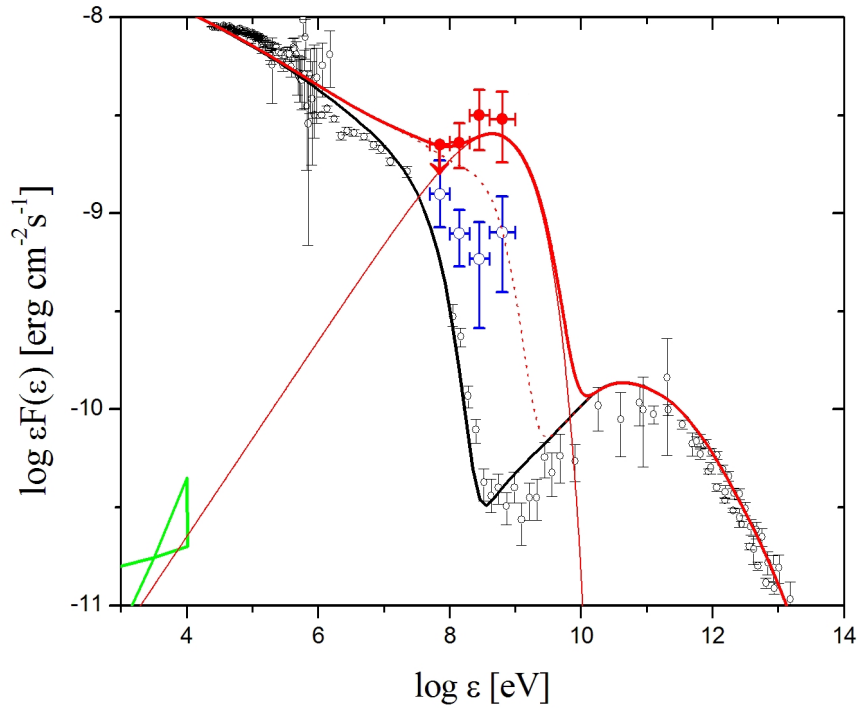
Figure 5: AGILE gamma-ray (pulsar subtracted) spectra of the Crab Nebula for the April 2011 super-flare (red points, 1-day integration) and for the September 2010 flare (blue points, 2-day integration) (from ref. [48]). Black data points show the standard Crab Nebula spectrum [37]. The area marked in green shows the X-ray emission spectrum detected by Chandra about 1 week after the Sept. 2010 flare from "Source A" in the inner Nebula as reported in ref. [51].
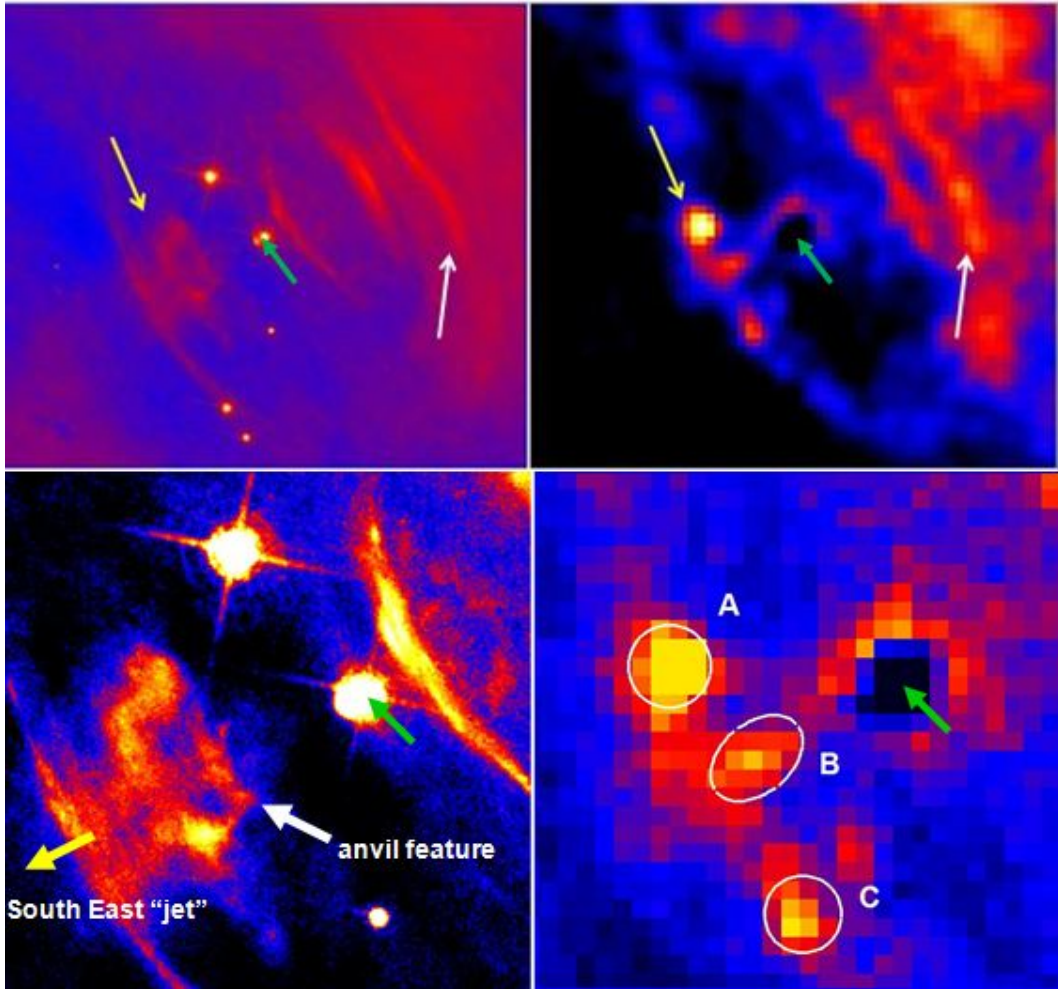
Figure 6: *HST* and *Chandra* imaging of the Crab Nebula following the Sept., 2010 gamma-ray flare (from ref. [51]). *Top left panel:* optical image of the inner nebula region (approximately 28"x28", North is up, East on the left) obtained by the *HST*-ACS instrument on October 2, 2010. ACS bandpass: 3,500-11,000 Angstrom. The pulsar position is marked with a green arrow in all panels. White arrows in all panels mark interesting features compared to archival data. *Top right panel:* the same region imaged by the *Chandra* Observatory ACIS instrument on September 28, 2010 in the energy range 0.5-8 keV (level-1 data). The pulsar does not show in this map and below because of pileup. *Bottom left panel:* zoom of the *HST* image (approximately 9"x9"), showing the nebular inner region, and the details of the "anvil feature" showing a "ring"-like structure at the base of the South-East "jet" off the pulsar. "Knot 1" at 0".6 South-East from the pulsar is saturated at the pulsar position. Terminology is from ref. [45]. *Bottom right panel:* zoom of the *Chandra* image, showing the X-ray brightening of the "anvil" region and the correspondence with the optical image. Analysis of the features marked "A", "B", and "C" gives the following results in the energy range 0.5-8 keV for the flux F, spectral index α, and absorption N_H (quoted errors are statistical at the 68% c.l.). Feature A: flux $F = (48.5 \pm 8.7) \cdot 10^{-12}\,\mathrm{erg\,cm^{-2}\,s^{-1}}$, $\alpha = 1.76 \pm 0.30$, $N_H = (0.36 \pm 0.05) \cdot 10^{22}\,\mathrm{atoms\,cm^{-2}}$. Feature B: flux $F = (26.6 \pm 5.9) \cdot 10^{-12}\,\mathrm{erg\,cm^{-2}\,s^{-1}}$, $\alpha = 1.76 \pm 0.41$, $N_H = (0.34 \pm 0.05) \cdot 10^{22}\,\mathrm{atoms\,cm^{-2}}$. Feature C: flux $F = (25.3 \pm 5.9) \cdot 10^{-12}\,\mathrm{erg\,cm^{-2}\,s^{-1}}$, $\alpha = 1.46 \pm 0.36$, $N_H = (0.34 \pm 0.04) \cdot 10^{22}\,\mathrm{atoms\,cm^{-2}}$.